PHYSICS AND CHEMISTRY OF SOLID STATE
V. 25, No. 4 (2024) pp. 892-902
Section: Technology

DOI: 10.15330/pcss.25.4.892-902

Vasyl Stefanyk Precarpathian National University

ФІЗИКА І ХІМІЯ ТВЕРДОГО ТІЛА
Т. 25, № 4 (2024) С. 892-902
Технічні науки

PACS: 61.46.Df; 61.72.uf

ISSN 1729-4428 (Print)
ISSN 2309-8589 (Online)

S. Levytskyi[1], Z. Cao[2], O. Koba[3], M. Koba[3]

Change of the Optoelectronic Properties of Semiconductor Compounds Induced by Nanosecond Laser Irradiation Pulses

[1]*V.E. Lashkaryov Institute of Semiconductor Physics NAS of Ukraine, Kyiv, Ukraine, levytskyi@ua.fm*
[2]*Institute of Physics and Technology, National Technical University of Ukraine "Igor Sikorsky Kyiv Polytechnic Institute", Kyiv, Ukraine*
[3]*Kyiv Institute of National Guard of Ukraine, Kyiv, Ukraine*

New research has discovered discrepancies in the melting points, plasma generation, and resulting changes in optoelectronic properties of semiconductor materials A_2B_6 and A_3B_5 when exposed to laser light, even when the experimental conditions are the same. Therefore, accurately determining the thresholds at which these complex semiconductor compounds melt and create plasma remains an unsolved task. This work utilizes nanosecond ruby laser irradiation to thoroughly examine fundamental characteristics of semiconductor compounds A_2B_6 and A_3B_5 when exposed to laser irradiation. This includes investigating the thresholds at which melting occurs, the production of plasma, and any changes in optoelectronic capabilities. The experimental results demonstrate notable discrepancies in the melting points and optoelectronic characteristics of various semiconductor materials when subjected to the same experimental conditions. The variations mostly arise from inherent statistical biases in the parameters of the sample. By employing photoacoustic and photoconductive techniques, we accurately ascertained the melting points of cadmium telluride, gallium arsenide, and aluminum gallium arsenide crystals, providing exact empirical data on the characteristics of these corresponding substances.

In addition, we performed photoconductive spectroscopy tests on cadmium telluride exposed to nanosecond ruby laser pulses. We noticed a significant impact of the creation of a tellurium layer on the photoconductivity. The investigations showed that the existence of a tellurium layer results in photoconductivity that varies depending on the spectrum, with the most significant improvement observed in the short-wavelength region.

Keywords: CdTe, GaAs, AlGaAs, laser irradiation, photothermal acoustic, photoconductive method.

Received 07 August 2024; Accepted 12 December 2024.

Introduction

The study of the auditory effects caused by laser radiation has gained significant attention in recent years. The attention is focused on investigating the diverse phenomena that occur when laser radiation interacts with matter. This attention is driven by both the need to understand these phenomena and their significant practical implications in optics, acoustics spectroscopy, and microscopy. Optoacoustics shows great promise in improving novel non-contact non-destructive testing techniques and wideband acoustic diagnostics for condensed materials. Within the field of semiconductors, specifically in single crystals of *CdTe*, the use of laser stimulation techniques provides the possibility to generate structures on the surface of the sample that possess precise optoelectronic characteristics. This capability allows for the production of many devices, including solar cells, X-ray and gamma-ray detectors, photodetectors, infrared filters, and other functional components. Due to the wide range of possibilities for using pulsed laser technology in manufacturing optoelectronic devices and instrument structures made from intricate semiconductor materials, it is crucial to accurately determine the threshold modes for laser-induced melting and plasma production.

The main physical mechanisms that cause sound to be generated when laser radiation interacts with matter include thermal-optical effects, electrostriction, sudden

changes in the state of the medium (such as melting, evaporation, and optical breakdown), optical pressure, and the generation of electron-hole plasma in semiconductors. The influence of each mechanism is contingent upon the strength of the laser radiation, the energy density within the medium, and the thermal and physical characteristics of the medium. The most efficient methods for absorbing media throughout a wide range of intensities, until reaching the point of optical breakdown, are thermal-optical effects and evaporation. Extensive theoretical and practical studies have been conducted in the scientific literature on several aspects of laser-induced sound excitation [1-4].

When laser radiation interacts with a condensed substance that absorbs it, a sequence of separate reactions occurs. After undergoing partial reflection at the interface, the incident radiation enters the substance and becomes absorbed by the surface layer. The thickness of the surface layer is inversely proportional to the absorption coefficient α. The energy that is absorbed proceeds via thermalization, resulting in alterations in the physical and chemical characteristics of the substance that is exposed to radiation. It is important to highlight that the extent of the region exposed to laser radiation is not limited by $1/\alpha$ or the depth at which heating occurs. This is because the pressure pulse created in the irradiated area extends to wider distances [5-9]. Optical breakdown happens when the incident radiation intensity reaches a specific threshold. During this procedure, concentrated plasma with a high density is generated in the central area. As a consequence of unrestricted frequency conversion, the plasma begins to assimilate light, leading to additional enhancements in the absorbed energy. The cavity undergoes thermal expansion, leading to a subsequent increase in temperature and the initiation of a shockwave. Visible sparks or incandescent spots can be noticed during the breakdown of dielectric materials, either directly or by capturing them on photographic plates [10]. Under conditions of low heat flux intensity, heat conduction has a notable impact, while incident radiation mostly functions to heat the item. If heat conduction is unable to efficiently disperse the incoming energy, the outer layer will rapidly increase in temperature and initiate evaporation. This will result in the redistribution of the incoming energy flow between the heat flow entering the object's interior and the heat flow used for material evaporation.

The occurrence of flash points resulting from plasma creation is unaffected by the composition and pressure of the surrounding gas, suggesting that the flash takes place within the vapor of the target substance. Plasma formation predominantly takes place at the forefront or upper part of the laser pulse, while the rear portion does not contribute to plasma production. The threshold intensity of laser flux for contaminated surfaces may be significantly lower, often 10 times or more, compared to that of clean surfaces. Contamination of the target surface leads to more intense evaporation, which in turn reduces the accuracy of theoretical estimations of applied stress intensity threshold. This is because the production of plasma always happens before the intense evaporation of the material. When the optical flux density is near the threshold, the region where it interacts with the medium shows boiling traces. These traces are seen as discrete pits, occasionally surrounded by a halo of solidified material droplets. Upon the emergence of a mature plasma cloud, it effectively absorbs the majority of the incoming optical energy, causing the previously confined energy release area to transition into a region of elevated pressure. Consequently, shockwaves and heating waves travel towards the optical energy. Optical absorption, in the meantime, takes place solely inside a limited area next to the shockwave, resulting in the conversion of the shockwave into a detonation wave. Afterwards, coherent rarefaction and heating waves arise and move towards the surface of the object. The shockwave rebounds off the solid surface, resulting in a delayed increase in pressure compared to the time at which the optical signal arrives. The pressure region in this process is considerably bigger than the area that is exposed to radiation on the surface of the target. During the extremely short duration of laser pulses, thermal diffusion occurs across a distance of a few micrometers, which is similar to or smaller than the distance over which light decays in semiconductors. The optical decay length in *Si* is 1.26 μm, in *GaAs* it is 0.787 μm, and in *CdTe*, it is 0.376 μm. These values are based on a wavelength of 0.5 μm for *GaAs* and 0.34 μm for *CdTe*.

Recent investigations have found notable discrepancies in the estimation of melting thresholds, plasma production, and the resulting alterations in the optoelectronic characteristics of semiconductor compounds A_2B_6 and A_3B_5 when exposed to laser light, even when the experimental conditions are comparable. The underlying reason for this situation is the unpredictable statistical variations in the characteristics of the analyzed samples, including dislocation density, doping agents, concentrations of different impurities, surface conditions, and so on. These causes result in substantial fluctuations in the recorded measurements.

We utilized photothermal acoustic (PTA) and photoconductive techniques. The photothermal acoustic method involves detecting thermal waves generated by modulated light as it interacts with a substance. The photoconductive approach is employed to assess and measure the newly generated states following laser therapy, both in terms of their quality and quantity. We do research on the stimulation of acoustic reactions, generation of plasma, and alterations in the photoconductive spectra of cadmium telluride when exposed to intense ruby laser pulses. In addition, we examined the internal friction forces that occur during the transportation of direct and alternating currents.

By employing these techniques, we can examine the sound reaction and creation of plasma in cadmium telluride, gallium arsenide, and aluminum gallium arsenide crystals when exposed to nanosecond ruby laser radiation. Additionally, we can ascertain the points at which these substances reach their melting limits.

I. Laser-induced modification of semiconductors and photoconductive methods

When A_2B_6 crystals, particularly *p-CdTe*, are exposed

to nanosecond ruby laser pulses at power densities below the point of fracture, changes occur both near the surface of the material and to a depth of around 5 μm, which is much greater than the optical absorption depth of α-105 cm-1. These changes cause alterations in the electrical, photoelectric, and optical characteristics [9-13]. The variations occur due to the development of inherent flaws within the crystal structure when it is heated, the creation of thermoelastic tension, and the impact of acoustic and shock waves.

Laser processing has emerged as a highly effective method for controlling semiconductor characteristics. The laser radiation quantum ($\hbar w$) can be adjusted to either surface properties ($\hbar w > E_g$) or bulk properties ($\hbar w < E_g$), depending on its ratio to the bandgap (E_g). The current understanding of the interaction mechanisms between laser irradiation and crystals is still insufficiently elucidated, despite substantial research [13, 14]. Prior studies [5, 15] observed the creation of a thin layer of tellurium on the surface of cadmium telluride when exposed to a ruby laser with specified pulse power. These studies also examined the photovoltaic characteristics of this tellurium film. The surface states during laser irradiation were examined by References [9-12] using photoconductive techniques.

Photoconductivity, sometimes referred to as the photoresistive effect, refers to the increase in electrical conductivity of a material when it is exposed to electromagnetic radiation in the visible, infrared (IR), or ultraviolet (UV) ranges. Photo current refers to the amplification of electric current in a complete circuit with a charged voltage source when a semiconductor is exposed to light. The magnitude of the photo current can greatly exceed that of the dark current. The fundamental principle of photoconductivity is the transmission of energy from photons to electrons through absorption. Following the absorption of photons by bound-state electrons in fully occupied valence bands or solids, electrons have the ability to move in response to an applied voltage. Photoconductivity is classified into two categories: unipolar, which involves either electrons or holes, and bipolar. It is determined by the charge polarity of the photo carriers. Intrinsic photoconductivity refers to the process in which electrons are excited and transferred from the valence band to the conduction band. On the other hand, impurity photoconductivity occurs due to the presence of localized electron levels. The photoconductivity's magnitude and time variations are contingent upon the intensity (I) and spectrum content of the excitation light, as well as the relaxation mechanisms of photo carriers. Excited photons must possess a sufficiently high energy to facilitate the movement of electrons from the valence band or other bound electron levels to the conduction band or free carrier state. Every transition corresponds to a certain wavelength line or band that is associated with stimulated photoconductivity. The concentration of photo carriers under constant light exposure is calculated using the equation $n = \eta\alpha I\tau$, where α represents the absorption coefficient (for uniform absorption, the condition $\alpha d << 1$ must be satisfied, where d is the thickness of the sample); η denotes the quantum yield of photoconductivity, which indicates the proportion of absorbed photons that generate the excitation of charge carriers, and τ represents the effective lifetime of free carrier states determined by relaxation mechanisms. The finite lifespan of photo-generated current carriers (electrons, holes, polarons) is ascribed to their confinement within different defects (traps) or recombination. The rarely observed phenomenon of "negative" photoconductivity (σ) is associated with the extra capture of free carriers caused by the absorption of light. The fundamental equations for conductivity and conductivity gain are as follows:

$$\sigma = en(\mu_n + \mu_p) \quad (1)$$

$$\Delta\sigma = \sigma_{pc} = e\mu_n \Delta n + e\mu_p \Delta p \quad (2)$$

The optical conductivity is closely linked to the production of changes in the density of electrons (Δn) and the density of hole (Δp) that occur as a result of light absorption. Hence, there is a clear and direct relationship between the optical conductivity and the absorption of light. This statement highlights a definitive differentiation between the inherent optical conductivity, particularly in the region of absorption edge, and the optical conductivity linked to contaminants. Significantly, there exists the occurrence of exciton photoconductivity. Although excitons possess no net charge, they can undergo dissociation, leading to the creation of electrons and holes. The existence of exciton peaks in the photoconductive spectrum is closely linked to the exciton absorption spectrum. At elevated energy levels, the optical conductivity undergoes a decrease as a result of the reduced ability of light to penetrate.

$$\alpha = 10^5 \text{ -} 10^6 \text{ 1/cm}$$

$$d = 1/\alpha = 0{,}1\text{-}0{,}01 \text{ mm.}$$

Hence, the influence of the surface on conductivity outweighs the influence of volume. Furthermore, there is a significant concentration of faults on the surface. The equation that describes the absorption of radiation by semiconductor material is denoted as $\frac{dI}{dx} = -\alpha I$, where I signify intensity. The quantity of photons that have been absorbed is equivalent to $\frac{\alpha I}{h\nu}$. The number of electron-hole pairs formed by light is denoted as $G = \frac{\alpha I}{h\nu}\beta$, where $\beta \sim \beta(h\nu)$ represents the photoionization coefficient, which quantifies the production of electron-hole pairs per photon. The equation appears to be in the form of

$-\frac{d\Delta n}{dt} = R_n - G_n$. The equation

$\Delta\sigma = \frac{e\alpha I}{h\nu}\beta(\tau_n\mu_n + \tau_p\mu_p)$

describes the rate at which excited charge carriers are generated and recombined. R_n represents the recombination rate, whereas G_n represents the rate of charge carrier creation.

II. Experimental Procedure for Semiconductor Irradiation using a Ruby Laser

This study employed a typical semiconductor laser irradiation approach [8-15], using a ruby laser in Q-switching mode, and a modulator consisting of a mixture of alcohol and a synthetic copper concealed cyanide molecule. The energy of radiation quanta is represented by the symbol ħw, which has a value of 1.78 electron volts (eV) and corresponds to a wavelength of 693.25 nanometers (nm). The pulse duration, written as timp, is equal to 20 nanoseconds (ns), and the form of the pulse closely resembles a Gaussian distribution.

In the irradiation experiment (see Figure 1), the laser spot is accurately concentrated on the sample surface within an area of 1 to 2 square millimeters. The laser pulse power is precisely controlled by using an absorption filter, allowing for a power variation range of ΔI = 1.5-2 MW/cm^2. The oscilloscope precisely regulates the duration and power of the laser pulse. Prior study has identified three specific areas in the laser radiation intensity during the *CdTe* irradiation experiment, as indicated by previous studies [3-5]: 1) Pre-threshold zone (pre-melting) - Starting from a particular intensity threshold, a layer of *Te* film gradually detaches from the surface of the sample, purifying the surface as all contaminants on the surface evaporate or ionize. 2) Threshold zone - Surface melting has a spatial distribution resembling islands, where the initial layer of atoms undergoes ionization and evaporation. 3) Post-threshold zone - Melting occurs in the layer near the surface at a depth of $1/\alpha$, where $\alpha = 10^5$ cm^{-1} represents the radiation absorption coefficient for a wavelength of 693.25 nm. The duration and power of the pulse have a significant impact on the melting lifespan and characteristics. It is predicted that the melt lifetime is many tens of nanoseconds [16].

When the pulse intensity reaches 40 MW/cm^2, plasma initiation occurs, causing ablation and the significant evaporation of material from the exposed surface due to the incident radiation. After the melt solidifies, a surface layer is formed, which is amorphous and has different optical properties compared to the bulk material. Eventually, this surface layer undergoes crystallization. Irradiation is carried out in a systematic manner by accumulating doses, where the dose (D) is equal to the product of the intensity (I), the number of pulses (N), and the time (t).

$$D = I \cdot N \cdot \tau_{puls}. \quad (3)$$

Photoconductivity research methodology

Figure 2 depicts the basic diagram of the apparatus used to test the photoconductivity spectrum. The device functions based on synchronous detection, which involves the integration of a light flux modulator M (with a rotational frequency of 400 rpm), a DC amplifier, and a synchronous detector into the optical channel, as shown in the figure. The reference voltage is produced by the reference voltage sensor in conjunction with modulator M.

The ultimate signal is documented by the recorder. The radiation source, lamp L, provides light that is concentrated into the entrance slit of the MDR-3 monochromator using a lens system. A beam of light of a

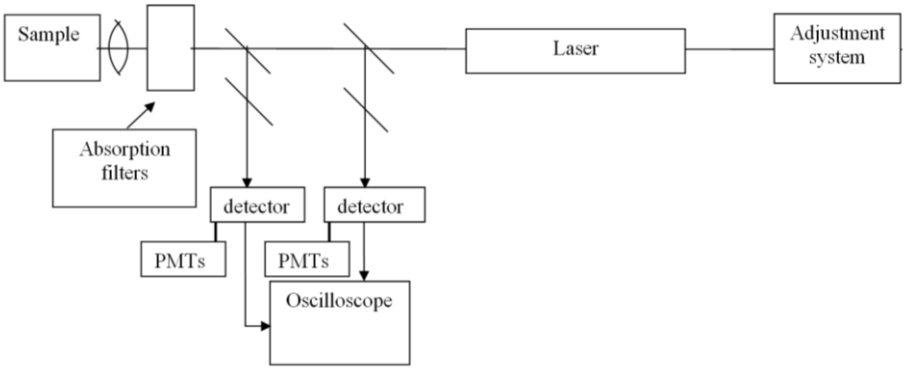

Fig. 1. Equipment frame of semiconductor irradiation with Ruby laser.

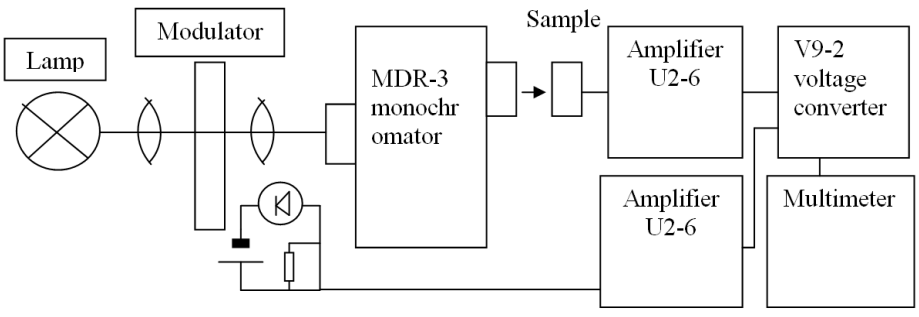

Fig. 2. Displays a schematic representation of the apparatus used to measure photoconductivity spectra.

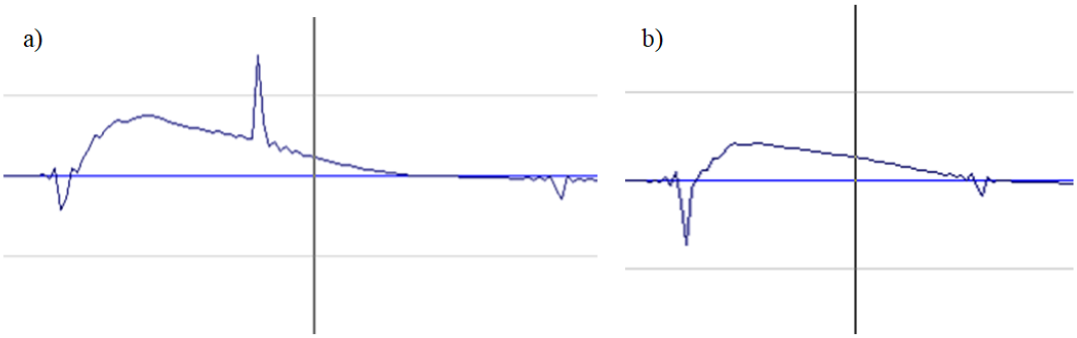

Fig. 3. a) Shows the flash duration and laser flash (indicated by the arrow) of the ruby laser pump lamp (13-15 microseconds). b) Shows the flash duration of the ruby laser pump lamp without generating laser light.

Fig. 4. The photodiode FD-7K records the plasma flash during the gallium arsenide irradiation process at different laser pulse intensities: 16 MW/cm^2 (a), 25 MW/cm^2 (b), 40 MW/cm^2 (c).

particular wavelength is projected onto the sample from the output of the monochromator, causing a photocurrent to be generated. After being amplified by amplifier U2-6 and sent by converter V9-2, the signal is then fed into the Multimeter. The light emitted by the light-emitting diode is sent to the photodiode PD I, which is part of an optocoupler. This generates a reference voltage for converter V9-2, ensuring synchronization.

III. Samples

The samples consist of *CdTe* (E_g = 1.42 eV), *Si* (E_g = 1.12 eV), *GaAs* (E_g = 1.5 eV), and *AlGaAs*/*GaAs*. The laser wavelength conditions, specifically $\hbar\omega < E_g$, indicate that the laser light is absorbed by the surface layer measuring 0.1-1 μm. The *CdTe* samples consist of p-type single crystals with orientations along the <*110*> and <*111*> directions (flake *CdTe*). The resistances of the samples are 1 MΩ and 1.5 GΩ, respectively, and the typical dimensions of the *CdTe* samples range from 1 mm to 3 mm. The *GaAs* samples are fabricated by depositing thin films of *AlGaAs* onto *GaAs* substrates with a <111> orientation. The sample is of n-type with a concentration of $n = 10^{16}$, a thickness of 1 μm, and a resistance of 700 kΩ. The *GaAs* substrate exhibits a resistance in the range of 10^7-10^8 Ω and has an electron concentration of 10^{12}, indicating it is of n-type. The silicon sample is a commercially manufactured polished p-type wafer with a reflectivity of R=37 % and a resistivity of ρ= 9 Ω·cm. Orientation <*111*>.

IV. Results

Plasma production is detected when a pulsed laser irradiates the material. The laser sparks are captured by the photodiode FD-7K and the resulting signals are transmitted to the computer via the FD sound card. Nevertheless, the true duration of the laser pulse does not align with the scale depicted in Figure 3.

In order to fully eliminate the red spectrum of the flash, we employ the SZS-24 filter. The enclosed photodiode employs its geometric design to minimize scattered light of various characteristics. Nevertheless, the photodiode-based plasma flash detection system may not consistently capture the plasma threshold due to its limited sensitivity. Hence, we captured the plasma threshold by optical means. Plasma is the occurrence of dielectric breakdown, when the vapor of a substance is evacuated in a concentrated manner from the melted state above the surface of a crystal when the temperature T is equal to or greater than the melting temperature (Tmelt). At the melting range, the plasma on the surfaces of *CdTe*, *GaAs*, and *GaAlAs* crystals becomes significantly brighter, resembling a spot of low intensity. As the laser pulse intensity rises, both the brightness and the size of the plasma region likewise increase. As the laser power rises, the plasma's color intensifies, resulting in a whiter shade. When the intensity is high, the shape of the plasma cloud matches the area that is being irradiated (refer to Figure 5 -6).

Plasma formation can occur even if only a few number of oxide atom layers evaporate off the surface

Fig. 5. Picture of plasma flash points.

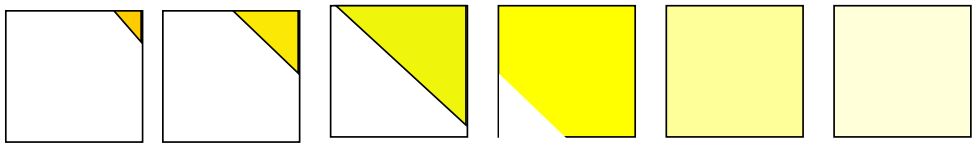

Fig. 6. As the value of I increases, plasma appears on the surfaces *CdTe* and *GaAs* ($I_1 < I_2 < I_3 < I_4 < I_5 < I_6$).

prior to melting. The initiation of plasma generation primarily relies on the surface treatment techniques employed and the level of cleanliness achieved. Research has indicated that the plasma threshold on newly obtained cadmium telluride samples aligns with the melting threshold of the chemical. The presence of low-intensity plasma prior to the melting threshold complicates the regulation of the melting threshold. At a power density of 7.97 MW/cm², we observed a marginal augmentation in the luminescence of untreated cadmium telluride samples (refer to Figure 7).

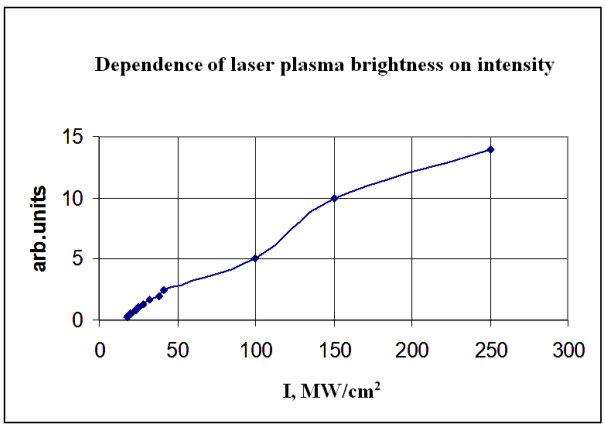

Fig. 7. Relationship between plasma brightness and intensity.

V. Investigation and examination of the factors that cause thermoacoustic excitation when exposed to laser light

The thermoacoustic excitation dynamics are mainly governed by radiation parameters, including spot size (a_0) and the relationship between a_0 radiation intensity and time ($I_{(r,t)}$), as well as the physical properties of the irradiated medium, such as compressibility (K). When the thermal radiation conditions are ideal, the thermal elastic stress produced in the medium can be approximately calculated using the expression $P \approx (\beta_t \cdot c_{sound}^2/2 \cdot c_p)E_v$. In this context, c_{sound} represents the velocity of sound, Ev is the volumetric density of absorbed light energy, and $(\beta_t \cdot c_{sound}^2/2 \cdot c_p)$ is a dimensionless value associated with the Gruneisen constant, which has an approximate order of 1. The conversion of energy into acoustic energy is directly proportional to the volume density of thermal emission, denoted as η. This may be calculated using the equation $\eta = E_{ac}/E_{sound} = (\beta_t \cdot c_{sound}^2/2 \cdot c_p)E_v/\rho_0 \cdot c_{sound}^2$, where ρ_0 represents the density of the medium. The data are shown in Tables 1, 2.

Table 1.

Data used for theoretical calculations of thermal stress in semiconductors under pulsed laser irradiation

	data are in degrees K		data are in degrees C	
	GaAs	***GaAs***	***GaAs***	***GaAs***
β, 1/K	$1.65 \cdot 10^{-5}$	$1.50 \cdot 10^{-5}$	$1.72 \cdot 10^{-5}$	$7.80 \cdot 10^{-6}$
$c_{звуку}$ m/s	3300	5000	5000	8430
c_p, J/kg*K	209	163.3	330	700
constant	$4{,}30 \cdot 10^{-1}$		$6.51 \cdot 10^{-1}$	$3.96 \cdot 10^{-1}$

Table 2.

Data for theoretical calculation of absorbed heat $E_v = (1\text{-}R) \cdot I \cdot \alpha \cdot \tau$.

	CdTe	***GaAs***	***Si***
α, 1/m	2940000	2000000	238000
A=(1-R)	0,564	0,66	0,66

The thermoelastic mechanism of acoustic excitation in condensed matter is constrained by the initiation of

evaporation under laser irradiation, rendering the absorption of energy beyond the evaporation threshold insignificant. The sound efficiency of thermoacoustic technologies is less than $\eta < 10^{-4}$. Nevertheless, the dense composition and intense heat generated by lasers interacting with solids enable the production of sufficiently potent sonic waves throughout a broad spectrum of frequencies.

The results of calculations are shown in Figures 8-10.

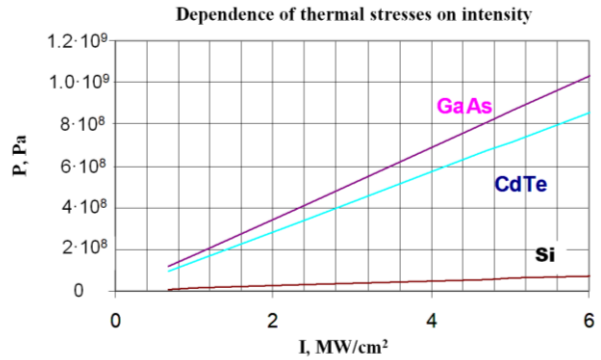

Fig. 8. Theoretical calculation of thermal stress on the crystal surface under pulsed irradiation.

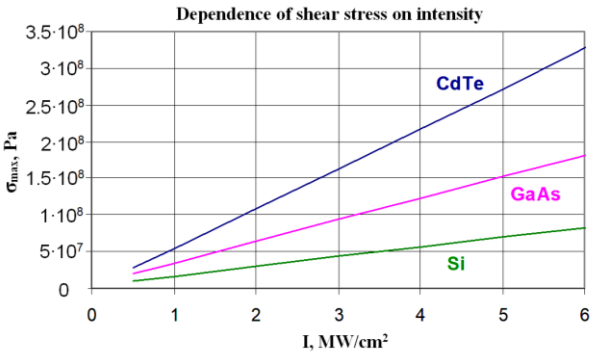

Fig. 9. Theoretical calculation of thermal shear stress on the crystal surface under pulsed irradiation, $\sigma_{max} = \alpha \cdot t \cdot G \cdot \Delta T \cdot (1-\mu)^{-}$.

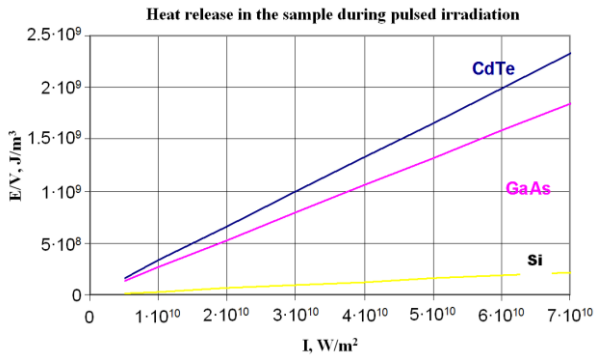

Fig. 10. Heat release from the near-surface layer of a crystal under laser irradiation as a function of intensity $E_v = (1-R) \cdot I \cdot \alpha \cdot \tau$

The maximum temperature in the pulse laser excitation area can be determined using the formula $T = \frac{IA}{\lambda\sqrt{K\pi}} arctg(\sqrt{4K\chi\tau})$, where $K=2/r_0^2$. Here, r_0 represents the characteristic beam size, I stands for intensity, A represents the absorption coefficient, λ represents thermal conductivity, χ represents thermal diffusivity, and τ represents the duration of the laser pulse. According to literature calculations[17], the laser irradiation of 8 MW/cm^2 causes the crystal surface temperature to exceed the melting point, as shown in Table 3.

Table 3.

I, *MBm/cм*^{2}	T, *K*	ΔT=T-300, *K*	σ_{max}, MPa
0	300	0	
0.5	380	80	18.9
1	444	144	34
2	487	187	53
4	976	676	107
5	1220	920	134
6	1464	1164	160
8			

VI. Analysis of the experimental results pertaining to photoconductivity.

Figure 11 exhibits the photoconductive spectrum of *CdTe* crystals. The spectra of the original sample displays distinct bands, with a maximum intensity at λ_{max} = 845 nm, which is in line with the width of the bandgap. Following irradiation with a ruby laser pulse (with a power density of 2 MW/cm^2), the photoconductivity values exhibit a rise, however the specific form and position of the maximum remain unaltered.

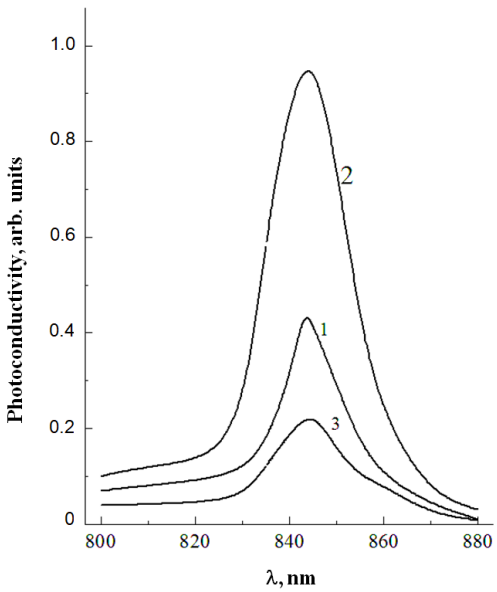

Fig. 11. Spectral dependence of photoconductivity of p-CdTe crystals: 1 - Untreated sample; 2 - after irradiation with a ruby laser pulse at 4 MW/cm^2; 3 - irradiated when the irradiation intensity reaches the tellurium evaporation threshold.

The formation of a tellurium layer occurs on the surface of cadmium telluride when it is exposed to

radiation. In order to confirm the connection between these modifications and the presence of the tellurium layer, we conducted a meticulous cleaning process on the cadmium telluride samples that had been exposed to radiation. This involved using a methanol solution containing 1 n KOH to clean each layer individually. Following a 10-minute rinse period, a reduction in photoconductivity values was noted. Additionally, when the tellurium film was exposed to laser pulses at or above the threshold intensity of 7 MW/cm^2, it evaporated. Following three wash cycles, the tellurium film fully regained its original properties. Hence, it can be inferred that the alterations observed in photoconductivity values during the irradiation process are a result of the creation of a *Te* layer on the surface of *CdTe*. Put simply, the presence of a tellurium layer that develops on the surface of cadmium telluride when exposed to laser radiation affects the way photoconductivity depends on the wavelength of light. The most significant enhancement in photoconductivity is observed in the shortwave area of the electromagnetic spectrum. This phenomenon can be attributed to the decrease in the rate at which charged particles recombine on the surface following exposure to radiation, resulting in alterations in the lifespan of charge carriers that are not in equilibrium. This phenomenon has been verified by investigations into the kinetics of photoconductivity in both pristine *CdTe* films and *CdTe* films that have been exposed to nanosecond ruby laser pulses.

The creation of a *Te* film on the surface of *CdTe* occurs due to the heating of the *CdTe* surface to a specific temperature under the influence of intense laser radiation. At this temperature, one of the constituent elements of the complex (often cadmium) has the potential to undergo melting and vaporization. Tellurium has a greater evaporation temperature and it remains in an amorphous state on the surface. Put simply, cadmium is more prone to vaporization than tellurium and will therefore evaporate from the surface before tellurium does. Upon reaching a specific threshold, the intensity will cause tellurium to undergo evaporation.

The photoconductive spectrum is significantly affected by surface characteristics, such as the existence of an oxide deposit, etching, and processing properties (level of polishing). The peak is associated with the absorption occurring in close proximity to the bandgap. The peak wavelength for cadmium telluride is around 845 nm, which corresponds to a photon energy of 1.46 eV. It should be noted that this value is an approximation, as impurity states are typically found near the band. The broadening is associated with the presence of an impurity layer located near the valence and conduction bands, which possesses a certain density of states.

In our scenario, the tellurium layer that is produced on the irradiation surface undergoes amorphous formation due to the quick cooling of the melt. Subsequently, it gradually crystallizes. The band structure (energy spectrum) of amorphous semiconductors is well recognized to be notably distinct from that of crystalline semiconductors. It is characterized by a pronounced reduction in the density of states along the boundaries of the valence and conduction bands. The gap also encompasses states that are linked to the amorphous structure. The conductivity on the side with short wavelengths (high photon energy) is determined by surface states and the rate at which generation and recombination occur in the gap. At lower photon energies, the conductivity is influenced by levels located within the gap, which are associated with doping, uncontrolled contaminants, and amorphous structure. The expansion of the lines following irradiation can be attributed to the existence of several extra states within the energy gap, as well as the formation of additional states at the periphery of the cadmium telluride band subsequent to laser processing.

The rise in photocurrent (*I*, photoelectric current) can be attributed to the elevated conductivity of the tellurium film, resulting in a significant reduction in resistance within the near-surface layer. The gap of *Te* is widely recognized to be 0.33 eV, which is significantly less than the gap of *CdTe*. The augmentation of photocurrent within the crystal subsequent to laser irradiation is pivotal for the advancement of photoelectric detectors.

VII. The internal friction of CdTe during the transmission of direct and alternating currents.

In order to assess the relationship between the internal friction and the elastic modulus *E* of *CdTe* crystals following mechanical cutting and grinding at various temperatures, we utilized a composite piezoelectric vibrator operating at a frequency of approximately 116 kHz. Additionally, we employed a driving resonance oscillation technique with a frequency of around 2 kHz [1]. The trials were carried out in a vacuum environment with a pressure of at least 10^{-3} Pa, and the strain ε was around 10^{-6}. The internal friction had a maximum measurement error of 10%, but the measurement error for the relative change in elastic modulus did not surpass 0.1%. The experiment utilized cadmium telluride samples measuring 2x2x16 mm^3. In order to facilitate the flow of electric current through the sample, we applied a layer of indium paste, measuring 2 mm in width, to both sides of the sample. Additionally, we added indium paste to the top of the sample and proceeded to solder fine silver wires to the indium contacts.

By subjecting the sample to an electric current, we observed and evaluated the alterations in elastic modulus resulting from the current's influence, the thermal effects induced by it, and the subsequent changes in elastic modulus due to heating.

The experiment found that when the sample was heated to 85 K while a current was applied, the change in elastic modulus (ΔE) divided by the initial elastic modulus (E_0) was around 7.2%. Here, Eo represents the absolute value of the elastic modulus before the current passes through, and *E* represents the absolute value of the elastic modulus after the current passes through. At a temperature of 85 K, when there was no current flowing, the change in energy (ΔE) relative to the initial energy (E_0) was 4.2%. Hence, without considering any heating effects, the influence of current flow on the fluctuation of $\Delta E/E_0$ can be approximated to be 3%.

No correlation between internal friction and ultrasonic deformation amplitude was observed when there was no current passing and the ultrasonic deformation amplitude increased. Nevertheless, when the sample was subjected to a temperature of 370 K and a constant current of no more than 0.9 A, while maintaining a constant ultrasonic strain $\delta \approx 2.10^{-6}$, we observed a rise in internal friction when the current was raised, as depicted in Figure 12.

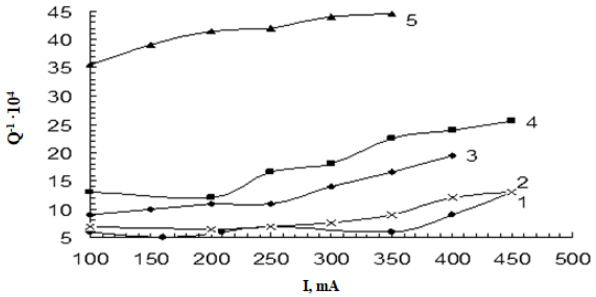

Fig. 12. Current dependence of internal friction in *CdTe* under constant ultrasonic deformation ($\delta \approx 2.10^{-6}$): 1 - 315 K, 2 - 335 K, 3 - 355 K, 4 - 365 K, 5 - 373 K.

The observed rise in internal friction depicted in Figure 11 can be attributed to the interaction between electrons possessing specific energy levels and oscillating dislocation segments, which occur as a result of ultrasonic deformation. This interaction prompts the dislocation segments to detach from point defects. The qualitative link between internal friction and direct current remains unaffected by the absolute value change of ultrasonic strain amplitude. However, it is worth noting that the range of ultrasonic amplitude fluctuation can exceed 5.10^{-6}. At a temperature of 470 K, an inverse relationship is observed between the critical value of direct current and temperature. By analyzing the fluctuation in the slope of the correlation curve between internal friction and current under a consistent ultrasonic strain, as shown in Figure 11, we can infer the presence of anchored dislocations. Therefore, the observed rise in the correlation between internal friction and current suggests the release of dislocations. The forward and reverse curves of the internal friction current exhibit full overlap, indicating the absence of any permanent alteration in the dislocation structure during the measuring procedure.

We conducted research on the impact of alternating current on internal friction while simultaneously subjecting the material to ultrasonic deformation. The signal generator G3-117 supplies both the alternating current that passes through the sample and is in phase with the voltage delivered to the piezoelectric vibrator, causing ultrasonic deformation. These two quantities are obtained from separate output terminals of the same signal generator.

Figure 13 demonstrates that when the alternating current reaches a critical value of approximately 50 mA, an augmentation in internal friction is evident, while the elastic modulus diminishes as the current increases. The study discovered that by altering the alternating current to match the voltage's frequency and phase, ultrasonic deformation occurs. Interestingly, the critical value of alternating current is nearly ten times smaller than the critical value of direct current. Observing the increase in internal friction with increasing direct current requires this condition to be met.

Hence, the impact of a consistent alternating current on the development of internal friction and the concomitant reduction in the magnitude of the elastic modulus has been observed in *CdTe* crystals. The detachment of oscillating dislocation segments from point defects is clearly caused by the electron flow during ultrasonic deformation.

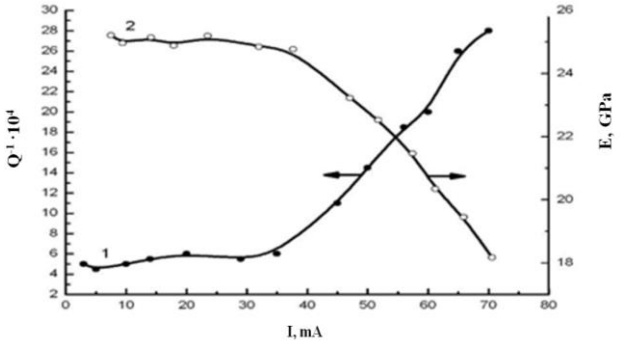

Fig. 13. The current relationship of the internal friction coefficient (1) and the elastic modulus (2) of *CdTe* with alternating current under the conditions of 294 K and constant ultrasonic strain ($\delta \approx 2.10^{-6}$).

VIII. Discussion

The research findings suggest that when exposed to nanosecond ruby laser pulses, the melting point of *CdTe* single crystal is reached at an irradiation intensity of 8 MW/cm^2, while the melting point of gallium arsenide is reached at an irradiation intensity of 6 MW/cm^2. The investigations demonstrate that the point at which plasma is formed on the sleek surface of cadmium telluride atoms aligns with its melting point. The study highlights that the purity and surface treatment method have an impact on the threshold for plasma production on *CdTe*, *GaAs*, and *AlGaAs* crystals. Oxides and other chemical compounds on the crystal surface reduce the minimum level required for plasma production.

The finding that the threshold for plasma generation on the sleek surface of cadmium telluride atoms aligns with the threshold for melting is highly significant. This association facilitates comprehension of the optical characteristics of *CdTe* and offers novel perspectives on its surface physical properties. The study indicates that the alignment between the melting point and the point at which surface plasma forms in *CdTe* reveals that intense energy input causes the disruption of the smooth atomic surface, resulting in its transformation into a plasma state. The relationship between *CdTe* and plasma state can possibly alter the optical properties of the former. This is because materials in a plasma state often demonstrate distinct optical characteristics compared to solid materials. Consequently, this alteration may have implications for the utilization of *CdTe* in optical devices. Studying the relationship between the threshold for plasma generation on the smooth surface of cadmium telluride and its melting threshold is highly important for comprehending its optical features and offers valuable insights for

investigating similar connections in other materials.

Moreover, the research suggests that the point at which plasma forms on the surfaces of *CdTe*, *GaAs*, and *AlGaAs* crystals is strongly influenced by the purity and type of surface treatment. This finding holds great importance for practical uses. The level of purity and the specific technique used for surface treatment have a direct impact on the threshold required for plasma generation. Implementing a high-purity surface treatment can decrease the occurrence of oxides and other chemical compounds, thereby reducing the threshold for plasma formation. Consequently, employing suitable surface treatment techniques can modify the chemical characteristics of the material surface, attain a reduced threshold for plasma generation, and facilitate the induction of a plasma state. By exercising control over surface treatment procedures, one may effectively regulate the chemical composition and morphology of the material surface. This is of utmost importance for the successful utilization of lasers, optical devices, and optoelectronics. Comprehending the influence of oxides and other chemical compounds on the threshold for plasma production is essential for developing surface treatment techniques customized to meet unique application demands.

It is imperative to acknowledge the constraints of the study. While this research offers insights into the relationship between the threshold for surface plasma production and surface treatment in *CdTe*, *GaAs*, and *AlGaAs* crystals, it is important to acknowledge its limits. Limitations such as constraints on sample range and treatment procedures, as well as the suitability of photoacoustic methods for material systems with low absorption or low optical power circumstances, restrict its usage. To enhance comprehension of this correlation, future research could investigate the following areas: broadening the study's scope to examine if comparable correlations exist between the threshold for surface plasma formation and surface treatment in different materials; conducting additional research and innovation to improve control over the chemical composition and morphology of material surfaces through new surface treatment techniques, and assessing their effect on the threshold for plasma formation; systematically examining the impact of experimental conditions on the threshold for surface plasma formation to gain a better understanding of the material's optical characteristics under varying conditions.

Subsequent investigations can go deeper into the mechanisms underlying these correlations, broadening the study's range to encompass more materials and surface treatment techniques. By undertaking these endeavors, we can acquire a more thorough comprehension of the electronic characteristics and optical efficacy of substances, thereby fostering the advancement of materials science and optical apparatus.

Levytskyi S. – Ph.D., Senior Research Fellow, specialist in optics of optoelectronic devices;
Cao Z. – Ph.D.student;
Koba O. – candidate of pedagogical sciences, deputy head of the department service and combat use of units of the National Guards of Ukraine;
Koba M. – senior lecturer of the Department of Legal Support service and combat activity.

[1] V.A. Gnatyuk, O.I. Vlasenko, S.N. Levytskyi, T. Aoki, *Electrical and photoelectric properties of M-p-n CdTe diodes*, Proceedings of The 6th International Conference on Global Research and Education: Inter-Academia 2007 and Inter-Academia for Young Researchers Workshop, 1, 446 (2007).
[2] S.V. Vinzents, A.V. Zaitseva, V.B. Zaitsev, G.S. Plotnikov, *Genesis of nanoscale defects and destructions in GaAs at multiple quasi-static photodeformation of micron regions of semiconductor*. FTP, 38(3), 257 (2004).
[3] A. Medvid', A. Mychko, V. Gnatyuk, S. Levytskyi, Yu. Naseka, *Mechanism of nano-cone formation on Cd0.9Zn0.1Te crystal by laser radiation*, Optical Materials, 32(8), 836 (2010); https://doi.org/10.1016/j.optmat.2010.03.006.
[4] A.L. Stepanov, V.N. Popok, D.E. Hole, A.A. Bukharev, *Interaction of powerful pulses of laser radiation with glasses containing implanted metallic nanoparticles*, 43(11), 2100 (2001).
[5] L.A. Golovan, P.K. Kashkarov, V.M. Lakeenko, V.Yu. Timoshenko, *Effect of pulsed laser irradiation on the optical characteristics and photoconductivity of solid solutions of CdHgTe*, 37(8), 931 (1997).
[6] P.O. Gentsar, O.I. Vlasenko, S.M. Levytskyi V.A. Gnatyuk, *Laser-stimulated increase reflectivity of semiconductors*, Physics and Chemistry of Solid State, 15(4), 856 (2014).
[7] A. Baidullaeva, V.P. Veleshchuk, O.I. Vlasenko, V.A. Gnatyuk, B.K. Dauletmuratov, S.N. Levytskyi, T. Aoki, *Mechanisms of mass transfer of indium in CdTe under nanosecond laser irradiation*, Ukrainian Journal of Physics, 56(2), 168 (2011); https://doi.org/10.15407/ujpe56.2.168.
[8] V.P. Veleshchuk, A. Baidullaeva, A.I. Vlasenko, V.A. Gnatyuk, B.K. Dauletmuratov, S.N. Levitskii, O.V. Lyashenko, T. Aoki, *Mass transfer of indium in the In-CdTe structure under nanosecond laser irradiation*, Physics of the Solid State, 52(3), 469 (2010); https://doi.org/10.1134/S1063783410030054.
[9] G.D. Ivlev, E.I. Gatskevich, V.A. Gnatyuk, V.P. Veleshchuk, A.I. Vlasenko, S.A. Dvoretskyi, N.N. Mikhailov, *Dynamics of the reflectivity of cadmium telluride based solid solutions under nanosecond laser action*, Proceedings of The IX International Scientific Conference "Laser Physics and Optical Technologies", Part 2, 171(2012).
[10] F.H. Mirzoev, V.Ya. Panchenko, L.A. Shelepin, *Laser control of processes in a solid body*, 166(1), 24 (1996).
[11] F.V. Bunkin, V.M. Komissarov, *Optical Excitation of Sound Waves*, Acoustic Journal, 19(3), 305 (1973).

[12] A.I. Vlasenko, V.P. Veleshchuk, V.A. Gnatyuk, S.N. Levitskii, Z.K. Vlasenko, G.D. Ivlev, E.I. Gatskevich, *Acoustic response to the action of nanosecond laser pulses on an In/CdTe thin-film heterostructure*, Physics of the Solid State, 57(6), 1089 (2015).
[13] V.E. Gusev, A.A. Karabutov. *Laser optoacoustics* (m. Science, 1991).
[14] S.P. Zhvavy, G.L. Zykov. *Numerical modelling of the dynamics of phase transitions in CdTe initiated by nanosecond excimer laser radiation*, FTP, 40(6), 652 (2006).
[15] P.O. Gentsar, O.I. Vlasenko, S.M. Levytskyi, V.A. Gnatyuk, M.S. Zayats, O.M. Strilchyk, Yu.M. Nasieka, *Optical properties of high-resistance CdTe single crystals and $Cd_{1-x}Zn_xTe$ solid solution*, Physics and Chemistry of Solid State, 13(4), 874(2012).
[16] S. M. Levytskyi, T. Zhao, Z. Cao, and A. V. Stronski, *Modeling of diffusion motion of in nanoparticles in a CdTe crystal during laser-induced doping*, Phys. Chem. Solid State, 22(2), 301(2021); https://doi.org/10.15330/pcss.22.2.301-306.
[17] V.P. Veleschuk, V.A. Gnatyuk, T. Aoki, Z.K. Vlasenko, S.M. Levytskyi, A.V. Shefer, A.G. Kuzmich, K.V. Dubyk, V.V. Kuryliuk, M.V. Isaiev, *Melting threshold and thermal conductivity of CdTe under pulsed laser irradiation*, in: A.R. Varkonyi-Koczy (eds) Engineering for Sustainable Future. INTER-ACADEMIA 2019. Lecture Notes in Networks and Systems, 101, 101 (2020); https://doi.org/10.1007/978-3-030-36841-8_10.

С. Левицький[1], Ц. Цао[2], О. Коба[3], М. Коба[3]

Зміна оптоелектронних властивостей напівпровідникових сполук під дією наносекундних імпульсів лазерного опромінення

[1]Інститут фізики напівпровідників ім. В.Є. Лашкарьова НАН України, Київ, Україна, levytskyi@ua.fm
[2]Фізико-техніний інститут Національного технічного університету України "Київський політехнічний інститут імені Ігоря Сікорського", Київ, Україна
[3]Київський інститут Національної гвардії України, Київ, Україна

Нові дослідження виявили розбіжності в температурах плавлення, утворенні плазми та, як наслідок, зміни в оптоелектронних властивостях напівпровідникових матеріалів A_2B_6 і A_3B_5 під дією лазерного світла, навіть якщо умови експерименту однакові. Тому точне визначення порогів, при яких ці складні напівпровідникові сполуки плавляться і створюють плазму, залишається невирішеним завданням. У даній роботі використовується наносекундне опромінення рубіновим лазером для ретельного вивчення фундаментальних характеристик напівпровідникових сполук A_2B_6 і A_3B_5 під дією лазерного опромінення. Це включає дослідження порогів, за яких відбувається плавлення, утворення плазми та будь-які зміни в оптоелектронних можливостях. Експериментальні результати демонструють помітні розбіжності в температурах плавлення та оптоелектронних характеристиках різних напівпровідникових матеріалів у тих самих експериментальних умовах. Варіації здебільшого виникають через властиві статистичні похибки в параметрах вибірки. Використовуючи фотоакустичні та фотопровідні методи, ми точно встановили температури плавлення кристалів телуриду кадмію, арсеніду галію та арсеніду алюмінію-галію, надаючи точні емпіричні дані щодо характеристик цих відповідних речовин.

Крім того, ми провели випробування фотопровідної спектроскопії на телуриді кадмію під впливом наносекундних імпульсів рубінового лазера. Ми помітили значний вплив створення шару телуру на фотопровідність. Дослідження показали, що існування шару телуру призводить до фотопровідності, яка змінюється залежно від спектру, причому найбільш значне поліпшення спостерігається в короткохвильовій області.

Ключові слова: CdTe, GaAs, AlGaAs, лазерне опромінення, фототермоакустика, фотопровідність.